






RESEARCH ARTICLE

Myfibroblast-specific inhibition of the Rho kinase-MRTF-SRF pathway using nanotechnology for the prevention of pulmonary fibrosis

 Rachel S. Knipe,^{1,2,3}  Md Nurunnabi,^{1,2,3} Clemens K. Probst,^{1,2,3} Jillian J. Spinney,^{1,2,3} Elizabeth Abe,^{1,2,3} Rajendran J. C. Bose,⁵  Khanh Ha,^{4,5} Amanda Logue,^{1,2,3} Trong Nguyen,^{1,2,3} Rachel Servis,⁶ Matthew Drummond,^{1,2,3} Alexis Haring,^{1,2,3} Patricia L. Brazee,^{1,2,3}  Benjamin D. Medoff,^{1,2,3*} and  Jason R. McCarthy^{4,5*}

¹Division of Pulmonary and Critical Care Medicine, Massachusetts General Hospital and Harvard Medical School, Boston, Massachusetts; ²Andrew M. Tager Fibrosis Research Center, Massachusetts General Hospital and Harvard Medical School, Boston, Massachusetts; ³Center for Immunology and Inflammatory Diseases, Massachusetts General Hospital and Harvard Medical School, Boston, Massachusetts; ⁴Center for Systems Biology, Massachusetts General Hospital and Harvard Medical School, Boston, Massachusetts; ⁵Biomedical Research and Translational Medicine, Masonic Medical Research Institute, Utica, New York; and ⁶Department of Pathology, Massachusetts General Hospital, Boston, Massachusetts

Abstract

Pulmonary fibrosis is characterized by the accumulation of myofibroblasts in the lung and progressive tissue scarring. Fibroblasts exist across a spectrum of states, from quiescence in health to activated myofibroblasts in the setting of injury. Highly activated myofibroblasts have a critical role in the establishment of fibrosis as the predominant source of type 1 collagen and profibrotic mediators. Myofibroblasts are also highly contractile cells and can alter lung biomechanical properties through tissue contraction. Inhibiting signaling pathways involved in myofibroblast activation could therefore have significant therapeutic value. One of the ways myofibroblast activation occurs is through activation of the Rho/myocardin-related transcription factor (MRTF)/serum response factor (SRF) pathway, which signals through intracellular actin polymerization. However, concerns surrounding the pleiotropic and ubiquitous nature of these signaling pathways have limited the translation of inhibitory drugs. Herein, we demonstrate a novel therapeutic antifibrotic strategy using myofibroblast-targeted nanoparticles containing a MRTF/SRF pathway inhibitor (CCG-1423), which has been shown to block myofibroblast activation in vitro. Myofibroblasts were preferentially targeted via the angiotensin 2 receptor, which has been shown to be selectively upregulated in animal and human studies. These nanoparticles were nontoxic and accumulated in lung myofibroblasts in the bleomycin-induced mouse model of pulmonary fibrosis, reducing the number of these activated cells and their production of profibrotic mediators. Ultimately, in a murine model of lung fibrosis, a single injection of these drugs containing targeted nanoagents reduced fibrosis as compared with control mice. This approach has the potential to deliver personalized therapy by precisely targeting signaling pathways in a cell-specific manner, allowing increased efficacy with reduced deleterious off-target effects.

cell-specific targeting; fibrosis; myofibroblast; nanoparticles; nanotechnology

INTRODUCTION

Idiopathic pulmonary fibrosis (IPF) is a progressive, debilitating disease that causes significant morbidity and mortality in affected patients. IPF is believed to result from dysregulated wound repair following lung injury (1). Central to this process is the activation and recruitment of lung fibroblasts to the alveolar structures. Once activated, fibroblasts transition into myofibroblasts which have a contractile phenotype and produce large quantities of collagen and other extracellular matrix proteins and fibrogenic mediators that lead to architectural distortion and dysfunction of the tissue. Prevention or reversal of the myofibroblast phenotype

has the potential to halt the progression of pulmonary fibrosis or even reverse established fibrosis and is thus a potential therapeutic approach in IPF.

Cytoskeletal signaling pathways have been implicated in the activation of myofibroblasts and therefore have a role in the development of fibrosis (2). One of the ways myofibroblast activation occurs is through activation of the Rho/myocardin-related transcription factor (MRTF)/serum response factor (SRF) pathway, which signals through intracellular actin polymerization. Consistent with this, MRTF-A (mkl1)-deficient mice are protected from bleomycin-induced pulmonary fibrosis (3). In addition, pharmacological inhibitors of MRTF have been shown to be protective in two different

*B. D. Medoff and J. R. McCarthy contributed equally to this work.

Correspondence: R. S. Knipe (rknipe@mgh.harvard.edu).

Submitted 11 March 2022 / Revised 19 October 2022 / Accepted 19 December 2022



mouse models of lung fibrosis via an increase in myofibroblast apoptosis (4).

Although the RhoA/MRTF/SRF pathway in fibroblasts has been shown to promote fibrosis, it is also an important homeostatic signaling mechanism for many cells. Therefore, global inhibition of this pathway may lead to impaired wound healing and tissue integrity. Cell-specific targeting, therefore, has appeal because it has the potential to target a profibrotic pathogenic cell type with reduced collateral damage. Herein, we describe the myofibroblast-specific localization of an inhibitor of MRTF (CCG-1423) via targeted nanoagents. To affect cell-specific internalization of these drug-loaded particles, we use a peptide-based ligand recognized by the angiotensin II type 2 receptor (AGTR2, ATII), the expression of which has been shown to be upregulated in IPF lung tissue and is localized to myofibroblasts, making it an ideal target for pulmonary fibrosis (5). These nanoagents demonstrate advantageous targeting profiles in vivo in the bleomycin-induced murine model of pulmonary fibrosis. Ultimately, the therapeutic efficacy of this strategy was investigated, demonstrating a reduction in collagen deposition with a single injection of the nanoparticle-encapsulated inhibitor at a dose that would otherwise be considered subtherapeutic.

MATERIALS AND METHODS

Generation of Fibroblast Targeted Nanoparticles

Details for the generation of the described nanoagents are included in the supplement, including synthetic procedures and compound characterization (Supplemental Figs. S1–S9; all supplemental material is available at <https://doi.org/10.6084/m9.figshare.21339084.v1>).

Bleomycin-Induced Pulmonary Fibrosis

C57BL/6 WT mice were purchased from Charles River Laboratories in Massachusetts. All mice were maintained in a specific pathogen-free (SPF) environment certified by the American Association for Accreditation of Laboratory Animal Care (AAALAC). All protocols performed were approved by the Massachusetts General Hospital Institutional Animal Care and Use Committee (IACUC). All experiments used male mice at 8 to 12 wk of age. C57BL/6 mice received standard dose intratracheal (IT) bleomycin (0.8 units/kg) after anesthesia (6, 7). Animal experiments were performed according to Animal Research: Reporting of *In Vivo* Experiments (ARRIVE) guidelines.

Biodistribution of Generated Nanoagents

At 10 d after bleomycin instillation, the nanoagents (ATII-targeted with drug, ATII-targeted without drug, or nontargeted with drug) were injected at 30 mg particle/kg (3 mg CCG-1423/kg) via the tail vein. Mice were euthanized 4 d later, and the organs were removed for fluorescence-based examination of biodistribution (Kodak ImageStation 4000, Carestream Health, Inc., Rochester, NY, excitation/emission 630/700 nm). Images were analyzed using ImageJ (v. 1.44o, Bethesda, MD).

Cellular Distribution of the Nanoagents Within the Injured Lung

At 10 d after lung injury, mice were injected with the nanoagents or respective controls at 30 mg particle/kg (3 mg CCG-

1423/kg) via the tail vein. Four days later, the animals were euthanized, and the lungs were removed and digested with an enzyme mixture of Liberase and DNase to yield a single-cell suspension. The suspension was stained with antibodies for CD45 (FITC), CD31 (PE), Epcam (BV605), and DAPI (PB), and subsequently subjected to flow sorting to give nanoparticle positive (CyAl5.5⁺) and negative cells in the fibroblast gate, using a negative selection gating strategy: CD45⁺ CD31⁺ Epcam⁺ cells.

Mouse Fibroblast Gene Expression

RNA was extracted from fluorescence-activated cell sorting (FACS)-isolated fibroblasts on *day 14* after IT bleomycin. RT-PCR was performed to quantify profibrotic gene expression, including CTGF. Primers were obtained from the Harvard/MGH PrimerBank.

Mouse Protein Expression

Protein was extracted from FACS-isolated fibroblasts on *day 14* after IT bleomycin. Proteins in whole lung lysates were resolved by SDS-PAGE and then transferred to nitrocellulose membranes using the NuPAGE electrophoresis and transfer systems (Life Technologies), under reducing conditions. After blocking with 5% milk, membranes were incubated with anti-CTGF antibody (1:2,000 dilution, rabbit IgG polyclonal, Thermo Fisher) followed by goat anti-rabbit secondary antibody (1:10,000 dilution, IRDye 800CW, Li-Cor), and images were obtained with the Li-Cor Odyssey CLx Imager. Membranes were then stripped and similarly re-probed with anti-GAPDH antibody (1:5,000 dilution, rabbit IgG polyclonal, Cell Signaling) as a loading control followed by goat anti-rabbit secondary antibody (1:10,000 dilution, IRDye 800CW, Li-Cor), and images were obtained with the Li-Cor Odyssey CLx Imager. Densitometry of the immunoblots was performed using Image J software (National Institutes of Health).

Determination of Therapeutic Efficacy

Cohorts of mice were injured as described in *Bleomycin-Induced Pulmonary Fibrosis*. At 10 d post-bleomycin, they were injected with the nanoagents (ATII-targeted with drug, ATII-targeted without drug, or nontargeted with drug) at 30 mg particle/kg (3 mg CCG-1423/kg), free CCG-1423 (3 mg/kg) in PBS/DMSO/ethanol or vehicle. At 4 d post-injection, the mice were euthanized, and the lungs were removed for the analysis of hydroxyproline content (6). Additional cohorts featuring the nanoagents were carried out to 28 d post-injury to determine survival and body weight curves.

Mouse Lung Histology

Separate cohorts of mice were treated as described in *Biodistribution of Generated Nanoagents*, for the biodistribution of generated nanoagents, with the lung tissue isolated for histologic analysis. Prior to excision, the right ventricle of the mouse and pulmonary vasculature were flushed with 10 mL cold PBS. The lungs were subsequently inflated with 10% buffered formalin at 25 cm H₂O for 10 min, excised and fixed in 10% formalin for 24 h, and then embedded in paraffin. Paraffin-embedded 5-μm sections were stained with hematoxylin and eosin or Masson's trichrome stains. For histological

analysis of nanoparticles, to preserve fluorescence, mouse lungs were freshly frozen in optimal cutting temperature (OCT) fixation compound. α -Smooth muscle actin (α SMA) staining (1:100 dilution, clone 1A4 monoclonal antibody, Sigma) was performed to visualize myofibroblasts in the lung tissue. Images were obtained on a Zeiss Widefield Microscope using Bright-field settings. Images were taken at $\times 10$ and $\times 20$ magnification.

Statistics

Descriptive analyses were conducted for the mice that received targeted nanoparticles with or without CCG-1423, and nontargeted nanoparticles with CCG-1423. Ranges and distributions were compared using the Kruskal–Wallis test to evaluate the differences of nanoparticles uptake by various organs, lung parenchymal cells, fibroblasts, as well as reduction in fibrosis and body weight at 28 days. We performed pairwise comparisons between group levels to assess which pairs of groups were different with Bonferroni corrections to account for multiple testing. To compare overall survival among groups of mice administered different nanoparticles, we used Kaplan–Meier curves to estimate the survival probability over time, and the log-rank test to compare the difference in survival functions across different groups. All statistical tests were two-sided, and $P < 0.05$ was considered statistically significant. All analyses were performed with RStudio software, v. 4.1.2.

RESULTS

Generation of Nanoagents for the Myofibroblast-Specific Inhibition of MRTF

Polymeric nanomaterials, in particular, those based on pegylated poly (lactic-co-glycolic acid) (PEG-PLGA) have been used extensively in the delivery of hydrophobic small molecule inhibitors. To enable their utility in the targeted delivery of inhibitors for the prevention of pulmonary fibrosis, the surface of the particle must be decorated in such a way to elicit uptake by the cell types of interest. To accomplish uptake by myofibroblasts within the lung, we conjugated a peptide-targeting ligand, RVYIHPI, to the surface of the nanoparticle. This peptide had been previously used to target the myocardium in a mouse model of myocardial infarction (8) and was found to co-localize well with α SMA-positive cells via binding to AGTR2. In addition to the modification of the particle surface with affinity ligands, we also include a near-infrared fluorophore (CyAl5.5) to enable the tracking of particle localization.

In this work, we use a water-in-oil emulsion technique to generate nanoparticles ~ 100 nm in size, with and without CCG-1423. For the targeted nanoagents, 10% of the polymer used is targeting peptide-modified, while an additional 10% is labeled with CyAl5.5. For the nontargeted particles, only the 10% CyAl5.5-labeled polymer was used, in addition to the base mPEG-PLGA. After centrifugal purification, the nanomaterials were subject to dynamic light scattering to determine hydrodynamic diameter (Fig. 1), whereas UV-vis spectroscopy was used to determine drug loading and release, with the particles demonstrating the inclusion of 10% drug, by mass. The drug release profile of CCG-1423

from the particles is shown in Supplemental Fig. S10. The drug-loaded materials exhibited an initial burst release of 28% during the first 24 h which can be attributed to the drug molecules embedded within the outermost layers or adsorbed onto the surface of the particle. After this initial burst, a more sustained release is observed, resulting in a 55% depletion of CCG-1423 from the nanomaterial by the fifth day. Mechanistically, encapsulated CCG-1423 release can be attributed to diffusion, polymer matrix erosion, swelling, and subsequent degradation of the PEG-PLGA polymer.

Myofibroblast-Targeted Nanoparticles Localize to the Fibrotic Lung after Bleomycin Challenge

To evaluate the targeting ability of nanoparticles *in vivo*, we used the bleomycin-induced pulmonary fibrosis mouse model. Intratracheal (IT) bleomycin was administered to C57BL/6 mice on *day 0* and then intravenous (IV) nanoparticles were injected on *day 10*. On *day 14*, after IT bleomycin, the liver, kidney, lung, heart, spleen, brain, and lymph nodes were harvested and imaged *ex vivo* to evaluate for the distribution of the nanoparticles (Fig. 2A). No significant uptake was seen in any organs with the administration of nontargeted nanoparticles. The targeted nanoparticles, on the other hand, clearly demonstrated excellent retention within the damaged lung (Fig. 2, B and C). As expected, fluorescence is also observed in the kidneys and the liver, which serve as the main points of clearance for nanomaterials and their degradation products.

Myofibroblast-Targeted Nanoparticles Are Specifically Taken up by Lung Fibroblasts after Bleomycin Lung Injury

To better define the cell-specificity of the nanoparticles, we again injured the lungs of WT mice with bleomycin and then injected nanoparticles IV on *day 10*, in the early stage of fibrotic remodeling. At *day 14*, a time point when there is established fibrosis, mouse lungs were harvested, digested to a single cell suspension, and sorted and quantified by flow cytometry hematopoietic cells (CD45⁺), endothelial cells (CD31⁺), epithelial cells (Epcam⁺), and fibroblasts (CD45[−]CD31[−]Epcam[−]) (Fig. 3A). Given that the nanoparticles are fluorescently labeled, particle positive and negative populations can also be defined. In these gated populations of lung cells, nanoparticles were only found in the lungs of mice that received targeted nanoparticles with or without CCG-1423 (Fig. 3, B–D). Among these four groups of lung parenchymal cells, the highest percentage of nanoparticle uptake was in the gate containing the fibroblast population with uptake in $\sim 6\%$ of the total isolated cells.

Myofibroblast-Targeted Nanoparticles Reduce Fibrosis in a Mouse Model of Disease

To test the therapeutic effects of fibroblast-targeted nanoparticles *in vivo*, we administered the nanoparticles to WT mice on *day 10* after IT bleomycin, and then monitored the body weight and health status of the mice for 28 days (Fig. 4A). There was no difference in weight loss and mortality in the mice that received nontargeted nanoparticles containing

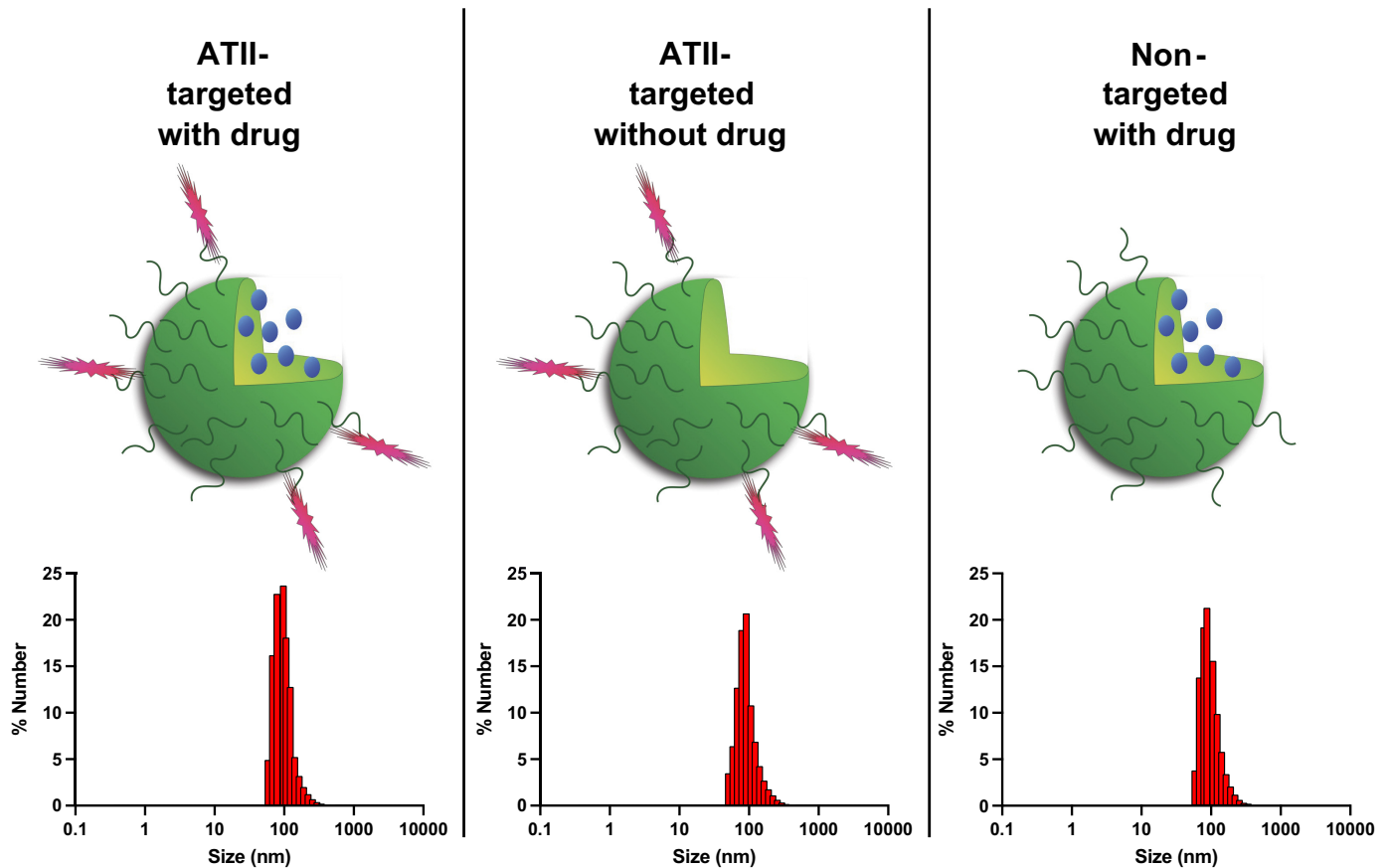


Figure 1. Characterization of myofibroblast-targeted nanoparticles. Schematics depicting the PEG-PLGA core (green) of each of the three nanoparticles generated for these experiments. In the targeted particles with drug (T + D), the core is coated with AGTR2-targeted peptides (purple) and contain CCG-1423 drug inside the shell (blue). In the targeted particles without drug (T – D), there is no CCG-1423 within the shell but the targeting peptide is seen on the outer shell. In the nontargeting particle with drug (NT + D), CCG-1423 is present within the shell but no targeting peptide is visible. Size distribution of the particles is shown below.

CCG-1423 compared with controls (Fig. 4B). We found a nonsignificant protective trend of the targeted nanoparticles containing CCG-1423 on survival compared with the other groups (overall test of the difference in survival probability across four groups $P = 0.356$, T + D vs. control $P = 0.194$, T + D vs. T – D $P = 0.136$, T + D vs. NT + D $P = 0.2$) (Fig. 4C). We also examined lung histology from WT mice on day 14 after IT bleomycin and compared mice that received targeted nanoparticles with or without CCG-1423, and nontargeted nanoparticles with CCG-1423. H&E and trichrome staining suggested a reduction in fibrosis in mice that received IV myofibroblast-targeted nanoparticles containing CCG-1423 as compared with those that received targeted particles without CCG-1423 and those that received nontargeted particles containing CCG-1423 (Fig. 4D). Pulmonary fibrosis was quantified by measuring hydroxyproline content in the lungs of WT mice on day 14 after IT bleomycin (day 4 after IV nanoparticles). There was a reduction in fibrosis in mice who received targeted nanoparticles containing CCG-1423 as compared with mice who received targeted nanoparticles without the drug and those that received nontargeting nanoparticles with CCG-1423 (Fig. 4E). IV administration of free drug CCG-1423 at the same dose as loaded in the nanoparticles was also administered on day 10 for comparison. This one-

time IV administration of CCG-1423 did not have the same effect on the reduction of pulmonary fibrosis as the drug-containing targeted nanoparticles (Supplemental Fig. S11).

Myofibroblast-Targeted Nanoparticles Reduce α SMA Staining in a Mouse Model of Disease

Mice that received nontargeted nanoparticles had minimal fluorescent particles visible in the lungs at day 14, consistent with the in vitro flow cytometry data demonstrating less uptake with the nontargeted nanoparticles (Fig. 5A). In mice that received targeted nanoparticles without drug, the particles co-localized with α SMA expressing regions of the lung, consistent with fibrotic regions containing myofibroblasts. In mice that received targeted nanoparticles loaded with CCG-1423, we saw regions of the lung with high concentrations of nanoparticle uptake and reduced expression of α SMA, suggesting a possible local drug effect, as CCG-1423 has been shown to induce fibroblast apoptosis and reduce fibrosis (4). To test the effect of the nanoparticles on gene expression, a fibroblast-enriched population of cells was isolated by FACS through negative selection gating ($CD45^-CD31^-Epcam^-$ cells) from mice on day 14 after IT bleomycin and IV nanoparticles (day 10). Fibroblasts that stained positive for nanoparticle uptake

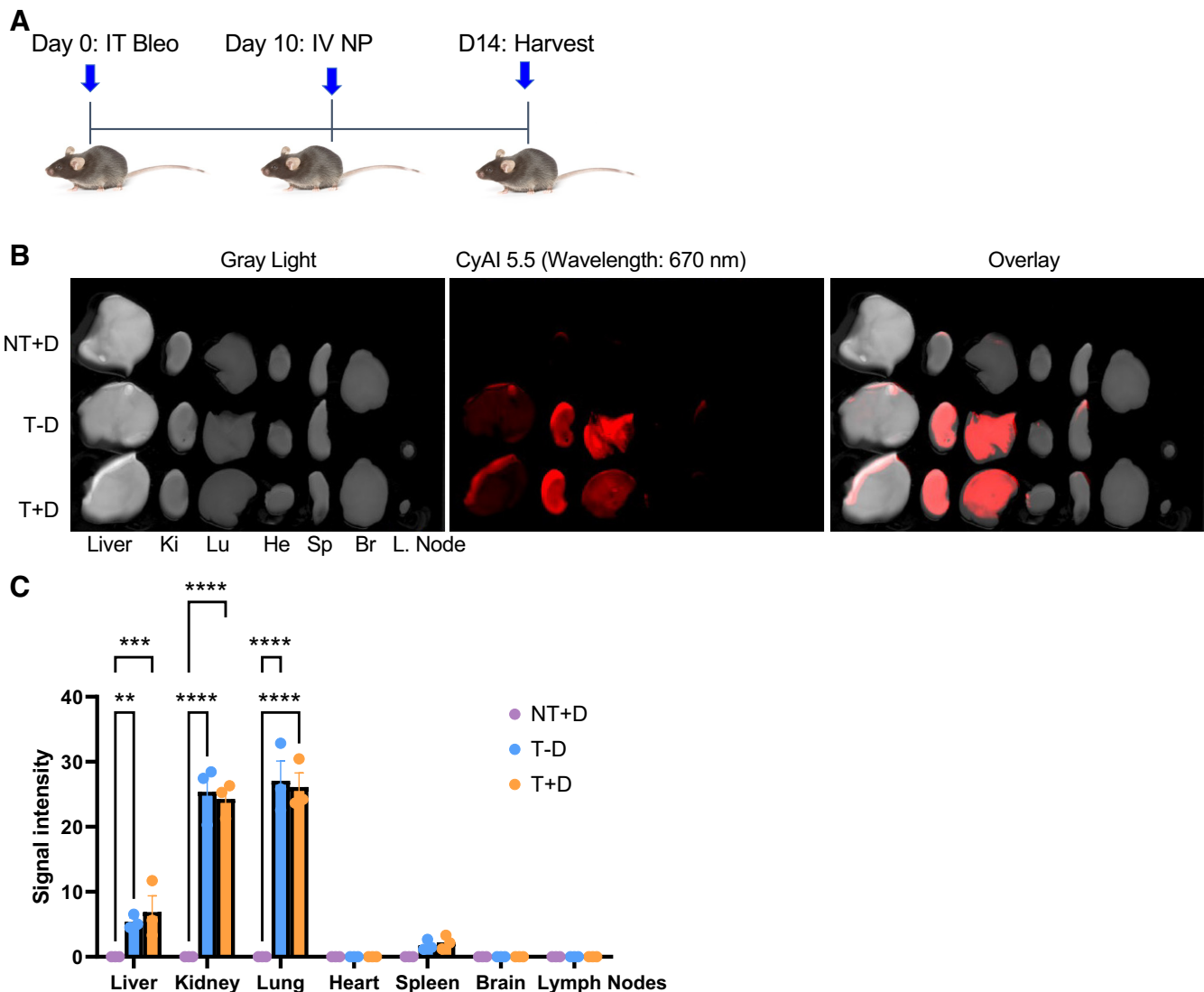


Figure 2. Ex vivo characterization of myofibroblast targeted nanoparticles after IT bleomycin. **A:** schematic of experimental design. C57BL/6 mice were injected with IT bleomycin (0.8 U/kg) on day 0, IV nanoparticles were injected day 10, and mouse lungs were harvested on day 14. **B:** ex vivo biodistribution demonstrated uptake of targeted nanoparticles in the lungs, kidney, and liver. **C:** quantification was performed of fluorescence uptake of organs ex vivo at day 14. $n = 3$ animals per group. NT + D, nontargeting nanoparticle with drug; T + D, targeting nanoparticle with drug; T – D, targeting nanoparticle without drug. ** $P < 0.01$, *** $P < 0.001$, **** $P < 0.0001$.

were sorted and collected. mRNA was extracted from the fibroblasts containing nanoparticles and RT-PCR was performed which demonstrated a reduction in the expression of the profibrotic mediator CTGF in mice treated with targeting particles containing drug as compared with those from mice treated with targeting particles without drug (Fig. 5B). Immunoblotting of mouse total lung homogenates collected at day 14 after IT bleomycin and IV nanoparticles (day 10) demonstrated reduced CTGF protein expression, consistent with a reduction in the levels of profibrotic mediators with cell-specific CCG-1423 administration (Fig. 5C).

DISCUSSION

IPF is characterized by persistent, progressive pulmonary fibrosis punctuated by episodes of acute exacerbations,

which are associated with significant morbidity and mortality (1). Despite two FDA-approved therapies, IPF remains a disease with a very poor prognosis and unpredictable clinical course (1). The two approved therapies for IPF, Nintedanib and Pirfenidone, only slow the rate of lung function decline and are associated with significant side effects (9, 10). Thus, there remains a critical need for novel therapies for IPF, ideally with minimal side effects.

This study was designed to investigate whether the targeted inhibition of MRTF specifically within activated myofibroblasts in the injured lung was sufficient to give an antifibrotic therapeutic effect. We reasoned that we could selectively target myofibroblasts using AGTR2, a receptor highly expressed on myofibroblasts but not on quiescent fibroblasts (5). This would allow normal fibroblasts to perform baseline homeostatic functions while targeting the pathologically activated myofibroblast population. Previous

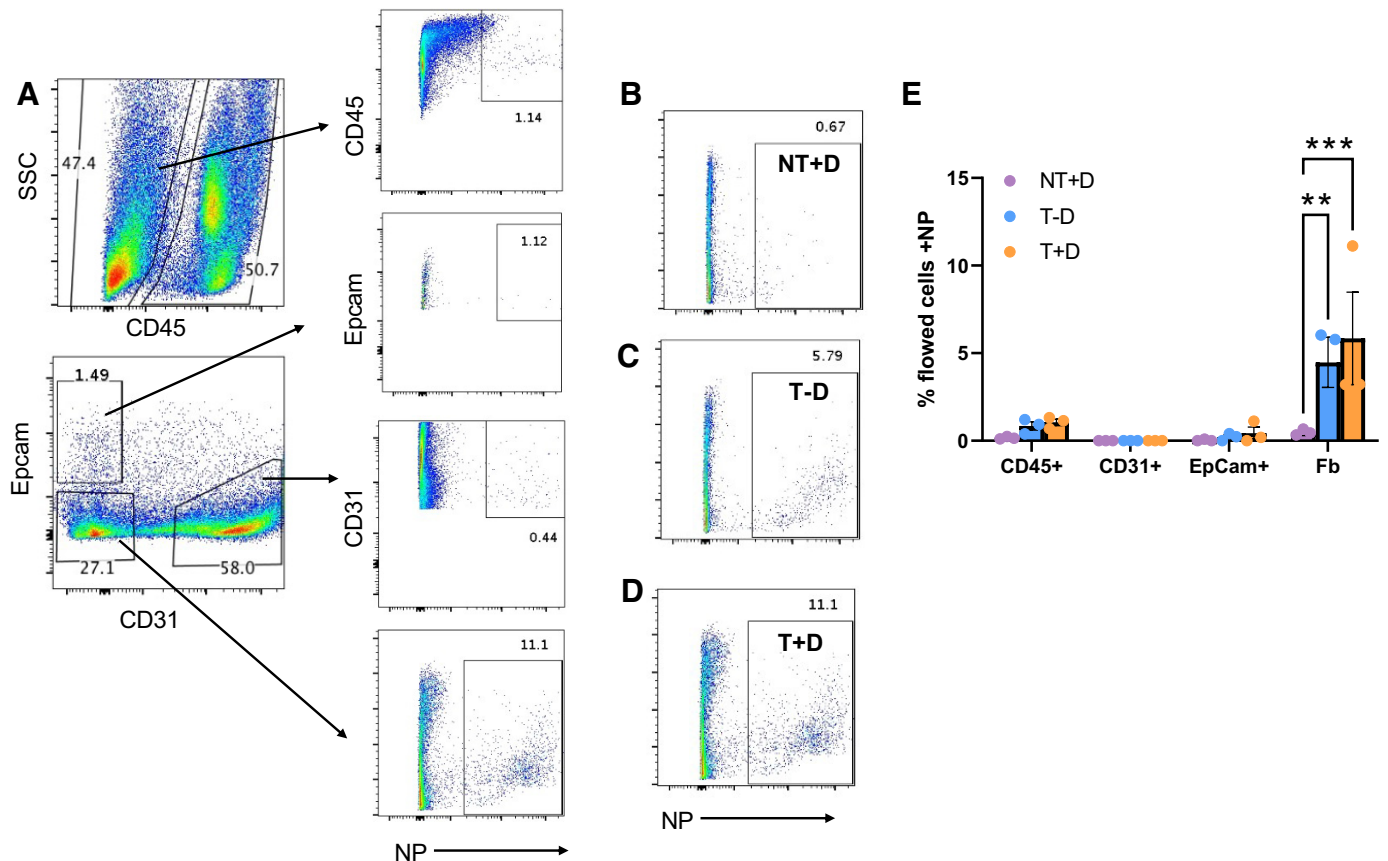


Figure 3. Myofibroblast targeted nanoparticles are specifically taken up by lung fibroblasts after lung injury with bleomycin. **A:** flow cytometry was performed on single cell suspension of lung tissue generated at day 14 after IT bleomycin. Hematopoietic cells (CD45⁺), epithelial cells (Epcam⁺), endothelial cells (CD31⁺), and fibroblasts (CD45⁻Epcam⁻CD31⁺) were identified through the gating strategy shown. **B:** nanoparticles were not well visualized in the lung fibroblasts by flow cytometry in mice who received IV nontargeting nanoparticles. In contrast, nanoparticles were well visualized by flow cytometry in the mice who received targeting nanoparticles without CCG-1423 (**C**) and in those who received targeting nanoparticles containing CCG-1423 (**D**). Representative images of $n = 3$ mice/group. **E:** nanoparticle containing cells were quantified for hematopoietic cells, endothelial cells, epithelial cells, and fibroblasts. $n = 3$ samples/group. NT + D, nontargeting nanoparticle with drug; T + D, targeting nanoparticle with drug; T - D, targeting nanoparticle without drug. ** $P < 0.01$, *** $P < 0.001$.

studies using MRTF inhibitor CCG-203971, a chemically modified derivative of CCG-1423, demonstrated that systemic administration of the drug at 100 mg/kg administered twice daily beginning on day 11 for 10 days after injury could provide a 35% of reduction in fibrosis (4). In contrast, we gave our model animals a single injection of CCG-1423 formulated in our targeted nanoagents at a dose of 3 mg/kg on day 10 after injury, an almost 700-fold overall reduction in dose, which resulted in a 15% decrease in fibrosis. A comparable 3 mg/kg dose of the free drug demonstrated no effect. This strategy has the potential to limit off-target effects and potential toxicity associated with the drug (11, 12), particularly through the reduced overall dosing and the cell-targeted nature of the vehicle design. As well, the myofibroblast-specific targeting limits the exposure of other cell types within the lung to the drug, mitigating the potential to block important homeostatic signaling of the Rho/MRTF/SRF pathway in other cell types such as epithelial cells, endothelial cells, and immune cells.

It is thought that a critical component of the pathogenesis of IPF involves recurrent injury to the alveolar epithelium accompanied by myofibroblast activation, leading to

aberrant lung tissue repair and deposition of the extracellular matrix (1). Therefore, the activation of myofibroblasts is a rational target for antifibrotic therapeutics. Myofibroblasts are characterized by increased proliferation, invasive capacity, resistance to apoptosis, and persistent secretion of collagen and other extracellular matrix proteins. In addition, myofibroblasts are highly contractile cells and can propagate mechanical stress on neighboring tissues, which may further expand profibrotic signals. Myofibroblasts do not play a significant role in normal tissue homeostasis, therefore they may serve as a therapeutic target to prevent further propagation of fibrosis and allow resolution of established disease.

The activation of myofibroblasts can be triggered by a variety of profibrotic mediators such as TGF- β and lysophosphatidic acid (LPA), both of which signal through the Rho/MRTF/SRF pathway (6, 13, 14). These stimuli activate this pathway through ligand binding of G-protein coupled receptors (GPCRs) at the cell surface (14). Activation of Rho/ROCK induces globular actin polymerization, which causes the release of MRTFs from their actin-bound state, potentiating translocation to the nucleus where they induce expression of profibrotic genes through activation of SRF (15). Previous

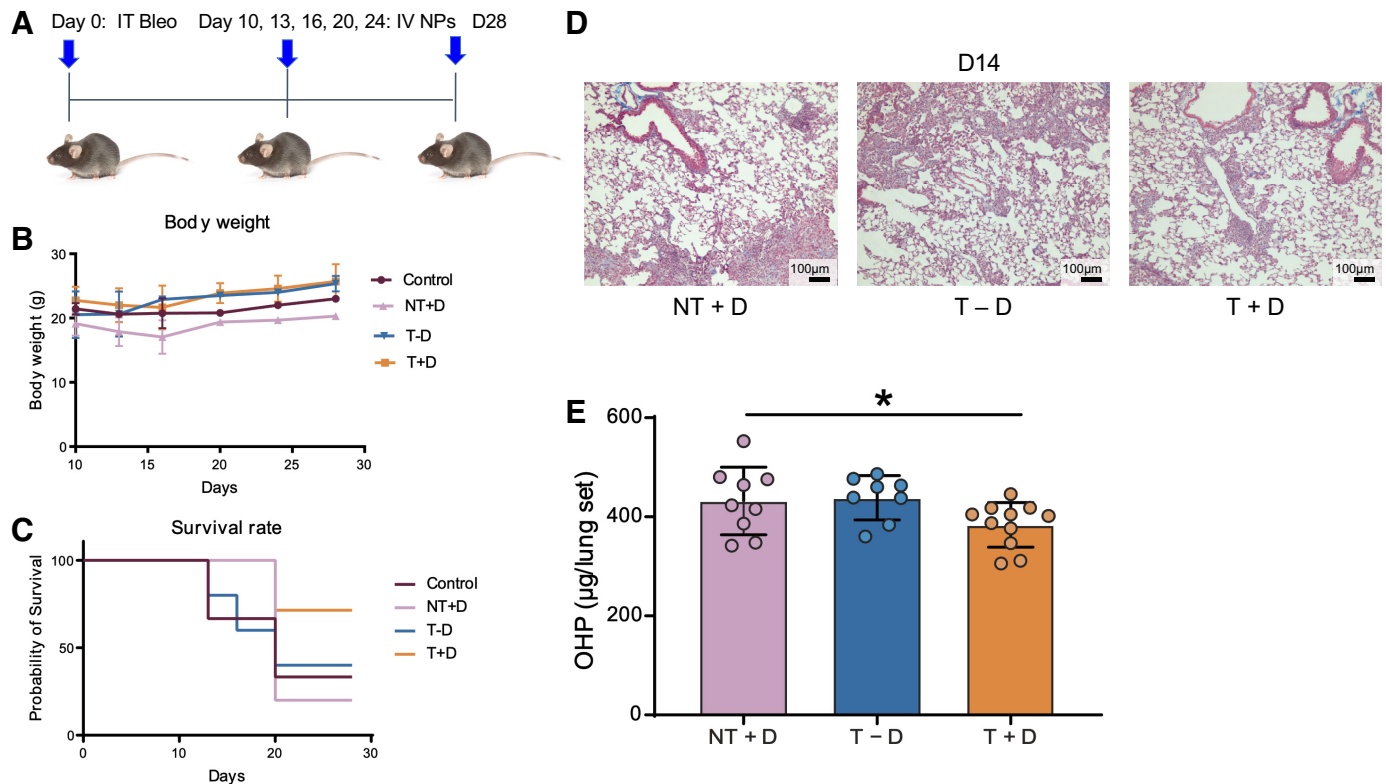


Figure 4. Myofibroblast targeted nanoparticles containing CCG-1423 attenuate bleomycin-induced pulmonary fibrosis. **A:** schematic of experimental design. C57BL/6 mice were injected with IT bleomycin (0.8 U/kg) on day 0, IV nanoparticles were injected on days 10, 13, 16, 20, 24 and mice were followed for 28 days. **B:** mouse body weight was measured at multiple time points over 28 days. **C:** survival was monitored over 28 days after IT bleomycin challenge. **D:** H&E staining was performed on mouse lung samples harvested on day 14 after IT bleomycin challenge. **E:** lung fibrosis was quantified by hydroxyproline assay on day 14 after IT bleomycin. $n = 8-11$ mice/group. $*P < 0.05$. NT + D, nontargeting nanoparticle with drug; T + D, targeting nanoparticle with drug; T - D, targeting nanoparticle without drug. $*P < 0.05$.

studies have demonstrated that inhibition of the Rho/MRTF/SRF signaling pathway prevents myofibroblast activation, promotes myofibroblast apoptosis, and limits the development of pulmonary fibrosis (4, 7, 13). However, in these previous studies, pathway inhibition was not cell specific, and in both in vitro and in vivo models of intestinal fibrosis, CCG-1423 demonstrated unacceptable cytotoxicity (12). In our own previous work focused on the modulation of Rho kinase isoforms ROCK1 and ROCK2 in pulmonary fibrosis, global deletion of either ROCK isoform in mice proved lethal, thus only those haploinsufficient for either ROCK isoform could be studied (16, 17). Mice haploinsufficient for either ROCK1 or ROCK2 were protected from bleomycin-induced pulmonary fibrosis (7). One of the mechanisms identified for this protective effect was a reduction in myofibroblast activation in the lung after bleomycin injury, as demonstrated by reduced α SMA staining of the lung tissue. In additional experiments, selective siRNA knockdown of ROCK1 or ROCK2 in human lung fibroblasts was also shown to reduce TGF- β -induced myofibroblast activation (7).

In our studies, the targeted nanoagents exhibited specific uptake in the injured lung, with secondary accumulation within the liver and kidneys. This is entirely expected as a clearance route for the materials retained within the tissue, with the lower molecular weight degradation products clearing through the renal system and the larger components through the hepatic system as they are slowly hydrolyzed

within the biological milieu and are removed from the lung. Our fluorescence-based biodistribution study was accomplished 48 h after injection, at which point the nontargeted particles have been cleared, demonstrating negligible signal as compared with the tissues containing the targeted materials. Within the lung, flow cytometry of single-cell suspensions of the tissues isolated from bleomycin-treated mice demonstrated that fibroblasts exhibited the largest percent uptake of nanoparticles. We chose to treat mice on day 10 after bleomycin administration at a time when fibrosis has already started in the lung and inflammation has waned (18). This may better reflect the therapeutic situation in patients with existing fibrosis. Importantly, there was evidence for reduction in myofibroblast activation with NP administration in these mice.

There are some apparent weaknesses in the methods used in the study. There are no antibodies available that adequately label mouse fibroblasts for identification and isolation via flow sorting. Our fibroblast population was contained within a triple negative gate, which is expected to encompass several stromal cell types. In this population, nanoparticles were only found in ~6% of the total gated cell population, which is most likely not indicative of their actual propensity to localize to the cells of interest. We also only investigated the injection of our drug delivery vehicles at a single time point and dose. Shifting the timing of injection to earlier or later time points may have profound effects on the therapeutic efficacy. As well, giving multiple

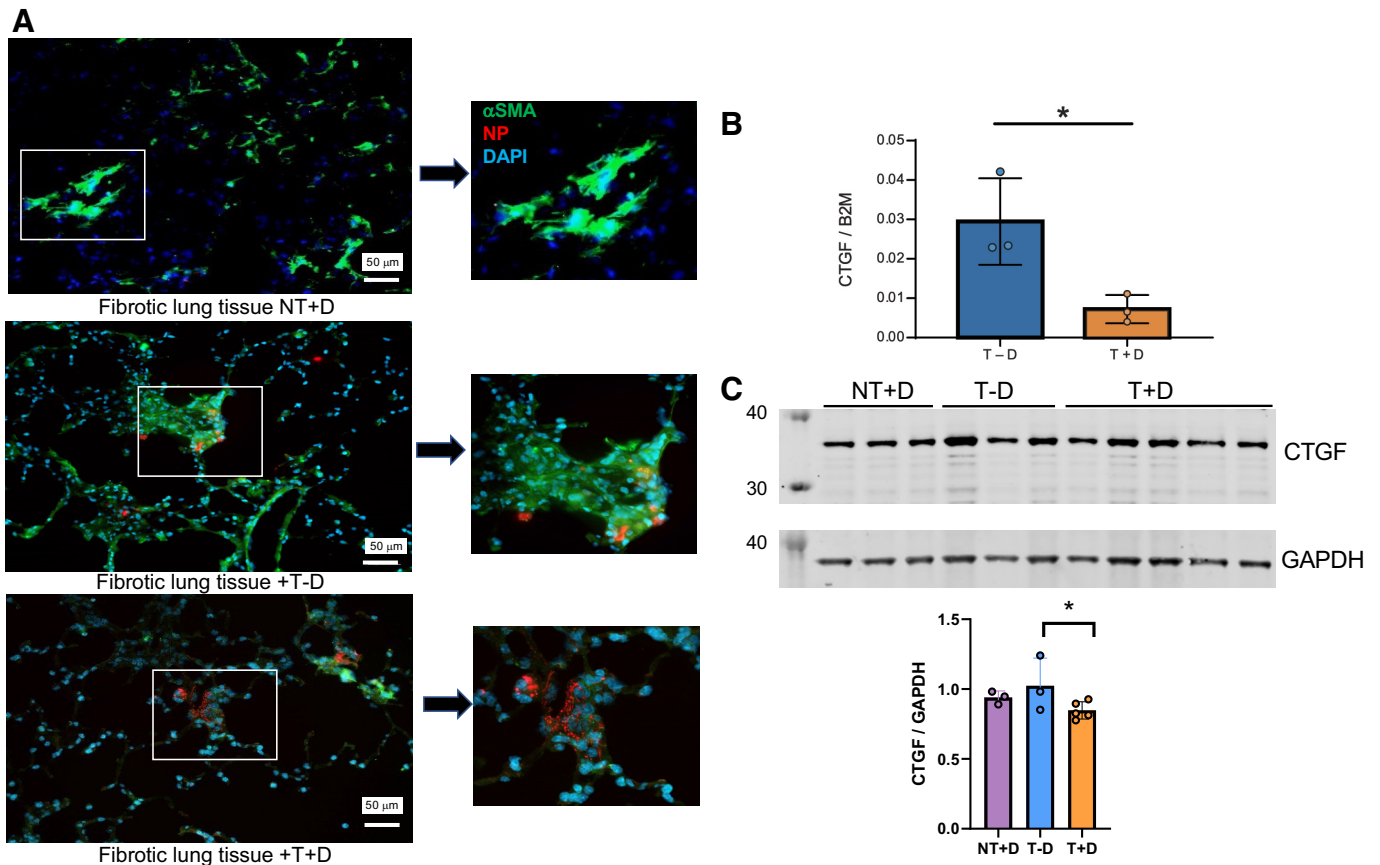


Figure 5. Myofibroblast-targeted nanoparticles containing CCG-1423 reduce myofibroblast activation. **A:** immunofluorescent staining was performed on mouse lung samples harvested on *day 14* after IT bleomycin challenge. Lung sections were stained for α SMA (green) and nanoparticles (red). Representative images shown. **B:** RNA was isolated from mouse lung fibroblasts containing nanoparticles and isolated by FACS at *day 14* after IT bleomycin. qPCR was performed to compare CTGF expression in fibroblasts containing targeted nanoparticles containing CCG-1423 to fibroblasts from mice containing targeted nanoparticles without CCG-1423. **C:** immunoblotting was performed on lung homogenates from mice treated with IV nanoparticles on *day 10* after IT bleomycin and probed for CTGF protein expression. $n = 4$ mice/group. NT + D, nontargeting nanoparticle with drug; T + D: targeting nanoparticle with drug; T - D, targeting nanoparticle without drug. $*P < 0.05$.

injections or increasing the apparent dose of the drug may increase the durability of the effect providing for an overall greater reduction in fibrosis.

In summary, these studies show for the first time that myofibroblast-targeted Rho/MRTF/SRF pathway inhibition delivered through nanoparticles to the lung can reduce bleomycin-induced pulmonary fibrosis with minimal side effects. Broadly, these findings suggest that targeted NPs may allow the safe delivery of drugs to specific pathogenic cell types while limiting effects on normal cells. These results expand the potential uses for drugs in development which may have different and undesirable downstream consequences in different cell types. Furthermore, the technology has the potential to facilitate the translation of results from preclinical studies using cell-specific genetically altered mouse models into clinical trials. Given the challenges of inhibiting important, fundamental signaling pathways that are active in both pathologic and homeostatic cells, cell-specific targeting is a potential solution to the problem by maximizing the on-target effects, such as reversing the myofibroblast phenotype, while limiting off-target effects, such as toxicity on regenerating epithelium or endothelium. Nanoparticles are already being used in

other disease processes such as cancer therapeutics, and thus could be used to target myofibroblasts and treat fibrotic diseases such as IPF.

DATA AVAILABILITY

Data will be made available upon reasonable request.

SUPPLEMENTAL DATA

Supplemental details for generation of nanoagents and Supplemental Figs. S1 and S2: <https://doi.org/10.6084/m9.figshare.21339084>.

ACKNOWLEDGMENTS

We acknowledge our colleague, mentor, and friend Dr. Andrew Tager for his inspiration on this project. We thank Dr. Susan Liu Sheng for edits and contributions to the figures and the manuscript. We thank Sophia Zhao for help with the statistical analysis for this project.

Present address of M. Nurunnabi: Dept. of Pharmaceutical Sciences, School of Pharmacy, University of Texas at El Paso, TX 79902.

GRANTS

These studies were supported by NIH Grant R01 HL133153 to B. D. Medoff and J. R. McCarthy and NIH Grant K08 HL140175 to R. S. Knipe.

DISCLOSURES

No conflicts of interest, financial or otherwise, are declared by the authors.

AUTHOR CONTRIBUTIONS

R.S.K., M.N., C.K.P., R.S., and J.R.M. conceived and designed research; R.S.K., M.N., C.K.P., J.J.S., E.A., R.J.C.B., K.H., A.L., T.N., R.S., M.D., A.H., and P.L.B. performed experiments; R.S.K., M.N., C.K.P., J.J.S., E.A., R.J.C.B., K.H., A.L., T.N., R.S., M.D., A.H., P.L.B., and J.R.M. analyzed data; R.S.K., M.N., C.K.P., J.J.S., E.A., R.J.C.B., K.H., A.L., T.N., R.S., M.D., P.L.B., B.D.M., and J.R.M. interpreted results of experiments; R.S.K., M.N., and J.R.M. prepared figures; R.S.K. and J.R.M. drafted manuscript; R.S.K., B.D.M., and J.R.M. edited and revised manuscript; R.S.K., M.N., B.D.M., and J.R.M. approved final version of manuscript.

REFERENCES

- Lederer DJ, Martinez FJ. Idiopathic pulmonary fibrosis. *N Engl J Med* 379: 797–798, 2018. doi:10.1056/NEJMc1807508.
- Santos A, Lagares D. Matrix stiffness: the conductor of organ fibrosis. *Curr Rheumatol Rep* 20, 2: 2, 2018. doi:10.1007/s11926-018-0710-z.
- Bernau K, Ngam C, Torr EE, Acton B, Kach J, Dulin NO, Sandbo N. Megakaryoblastic leukemia-1 is required for the development of bleomycin-induced pulmonary fibrosis. *Respir Res* 16: 45, 2015. doi:10.1186/s12931-015-0206-6.
- Sisson TH, Ajayi IO, Subbotina N, Dodi AE, Rodansky ES, Chibucos LN, Kim KK, Keshamouni VG, White ES, Zhou Y, Higgins PDR, Larsen SD, Neubig RR, Horowitz JC. Inhibition of myocardin-related transcription factor/serum response factor signaling decreases lung fibrosis and promotes mesenchymal cell apoptosis. *Am J Pathol* 185: 969–986, 2015. doi:10.1016/j.ajpath.2014.12.005.
- Königshoff M, Wilhelm A, Jahn A, Sedding D, Amarie OV, Eul B, Seeger W, Fink L, Günther A, Eickelberg O, Rose F. The angiotensin II receptor 2 is expressed and mediates angiotensin II signaling in lung fibrosis. *Am J Respir Cell Mol Biol* 37: 640–650, 2007. doi:10.1165/rcmb.2006-0379TR.
- Tager AM, LaCamera P, Shea BS, Campanella GS, Selman M, Zhao Z, Polosukhin V, Wain J, Karimi-Shah BA, Kim ND, Hart WK, Pardo A, Blackwell TS, Xu Y, Chun J, Luster AD. The lysophosphatidic acid receptor LPA1 links pulmonary fibrosis to lung injury by mediating fibroblast recruitment and vascular leak. *Nat Med* 14: 45–54, 2008. doi:10.1038/nm1685.
- Knipe RS, Probst CK, Lagares D, Franklin A, Spinney JJ, Brazee PL, Grasberger P, Zhang L, Black KE, Sakai N, Shea BS, Liao JK, Medoff BD, Tager AM. The Rho kinase isoforms ROCK1 and ROCK2 each contribute to the development of experimental pulmonary fibrosis. *Am J Respir Cell Mol Biol* 58: 471–481, 2018. doi:10.1165/rcmb.2017-0075OC.
- Verjans JWH, Lovhaug D, Narula N, Petrov AD, Indrevoll B, Bjurgert E, Krasieva TB, Petersen LB, Kindberg GM, Solbakken M, Cuthbertson A, Vannan MA, Reutlingsperger CPM, Tromberg BJ, Hofstra L, Narula J. Noninvasive imaging of angiotensin receptors after myocardial infarction. *JACC Cardiovasc Imaging* 1: 354–362, 2008. doi:10.1016/j.jcmg.2007.11.007.
- King TE, Bradford WZ, Castro-Bernardini S, Fagan EA, Glaspole I, Glassberg MK, Gorina E, Hopkins PM, Kardatzke D, Lancaster L, Lederer DJ, Nathan SD, Pereira CA, Sahn SA, Sussman R, Swigris JJ, Noble PW Jr, ASCEND Study Group. A phase 3 trial of pirfenidone in patients with idiopathic pulmonary fibrosis. *N Engl J Med* 370: 2083–2092, 2014 [Erratum in *N Engl J Med* 371: 1172, 2014]. doi:10.1056/NEJMoa1402582.
- Richeldi L, Du Bois RM, Raghu G, Azuma A, Brown KK, Costabel U, Cottin V, Flaherty KR, Hansell DM, Inoue Y, Kim DS, Kolb M, Nicholson AG, Noble PW, Selman M, Taniguchi H, Brun M, Le Mauff F, Girard M, Stowasser S, Schlenker-Herceg R, Disse B, Collard HR, INPULSIS Trial Investigators. Efficacy and safety of nintedanib in idiopathic pulmonary fibrosis. *N Engl J Med* 370: 2071–2082, 2014. doi:10.1056/NEJMoa1402584.
- Evelyn CR, Bell JL, Ryu JG, Wade SM, Kocak A, Harzdorf NL, Showalter HD, Neubig RR, Larsen SD. Design, synthesis and prostate cancer cell-based studies of analogs of the Rho/MKL1 transcriptional pathway inhibitor, CCG-1423. *Bioorg Med Chem Lett* 20: 665–672, 2010. doi:10.1016/j.bmcl.2009.11.056.
- Johnson LA, Rodansky ES, Haak AJ, Larsen SD, Neubig RR, Higgins PDR. Novel Rho/MRTF/SRF inhibitors block matrix-stiffness and TGF-beta-induced fibrogenesis in human colonic myofibroblasts. *Inflamm Bowel Dis* 20: 154–165, 2014. doi:10.1097/01.MIB.0000437615.98881.31.
- Sandbo N, Kregel S, Taurin S, Bhorade S, Dulin NO. Critical role of serum response factor in pulmonary myofibroblast differentiation induced by TGF-beta. *Am J Respir Cell Mol Biol* 41: 332–338, 2009. doi:10.1165/rcmb.2008-0288OC.
- Sakai N, Chun J, Duffield JS, Wada T, Luster AD, Tager AM. LPA1-induced cytoskeleton reorganization drives fibrosis through CTGF-dependent fibroblast proliferation. *FASEB J* 27: 1830–1846, 2013. doi:10.1096/fj.12-219378.
- Luchsinger LL, Patenaude CA, Smith BD, Layne MD. Myocardin-related transcription factor-A complexes activate type I collagen expression in lung fibroblasts. *J Biol Chem* 286: 44116–44125, 2011. doi:10.1074/jbc.M111.276931.
- Thumkeo D, Shimizu Y, Sakamoto S, Yamada S, Narumiya S. ROCK-I and ROCK-II cooperatively regulate closure of eyelid and ventral body wall in mouse embryo. *Genes Cells* 10: 825–834, 2005. doi:10.1111/j.1365-2443.2005.00882.x.
- Shimizu Y, Thumkeo D, Keel J, Ishizaki T, Oshima H, Oshima M, Noda Y, Matsumura F, Taketo MM, Narumiya S. ROCK-I regulates closure of the eyelids and ventral body wall by inducing assembly of actomyosin bundles. *J Cell Biol* 168: 941–953, 2005. doi:10.1083/jcb.200411179.
- Strunz M, Simon LM, Ansari M, Kathiriyi JJ, Angelidis I, Mayr CH, Tsidiridis G, Lange M, Mattner LF, Yee M, Ogar P, Sengupta A, Kukhtevich I, Schneider R, Zhao Z, Voss C, Stoeger T, Neumann JHL, Hilgendorff A, Behr J, O'Reilly M, Lehmann M, Burgstaller G, Königshoff M, Chapman HA, Theis FJ, Schiller HB. Alveolar regeneration through a Krt8⁺ transitional stem cell state that persists in human lung fibrosis. *Nat Commun* 11: 3559, 2020. doi:10.1038/s41467-020-17358-3.